Journal of Computational Mathematics
Vol.29, No.6, 2011, 623–638.

http://www.global-sci.org/jcm
doi:10.4208/jcm.1110-m11si02

HIGH ORDER WEIGHTED ESSENTIALLY NON-OSCILLATION SCHEMES FOR ONE-DIMENSIONAL DETONATION WAVE SIMULATIONS*

Zhen Gao
School of Mathematical Sciences, Ocean University of China, Qingdao 266100, China
Email: zhengao@ouc.edu.cn
Wai Sun Don
Department of Mathematics, Hong Kong Baptist University, Hong Kong, China
Email: wsdon@hkbu.edu.hk
Zhiqiu Li
Department of Mathematics, Hong Kong Baptist University, Hong Kong, China
Email: zhiqiuli@hkbu.edu.hk

Abstract

In this paper, three versions of WENO schemes WENO-JS, WENO-M and WENO-Z are used for one-dimensional detonation wave simulations with fifth order characteristic based spatial flux reconstruction. Numerical schemes for solving the system of hyperbolic conversation laws using the ZND analytical solution as initial condition are presented. Numerical simulations of one-dimensional detonation wave for both stable and unstable cases are performed. In the stable case with overdrive factor $f = 1.8$, the temporal histories of peak pressure of the detonation front computed by WENO-JS and WENO-Z reach the theoretical steady state. In comparison, the temporal history of peak pressure computed by the WENO-M scheme fails to reach and oscillates around the theoretical steady state. In the unstable cases with overdrive factors $f = 1.6$ and $f = 1.3$, the results of all WENO schemes agree well with each other as the resolution, defined as the number of grid points per half-length of reaction zone, increases. Furthermore, for overdrive factor $f = 1.6$, the grid convergence study demonstrates that the high order WENO schemes converge faster than other existing lower order schemes such as unsplit scheme, Roe's solver with minmod limiter and Roe's solver with superbee limiter in reaching the predicted peak pressure. For overdrive factor $f = 1.3$, the temporal history of peak pressure shows an increasingly chaotic behavior even at high resolution. In the case of overdrive factor $f = 1.1$, in accordance with theoretical studies, an explosion occurs and different WENO schemes leading to this explosion appear at slightly different times.

Mathematics subject classification: 65P30, 77Axx.
Key words: Weighted Essentially Non-Oscillatory, Detonation, ZND.

1. Introduction

Detonation is a complex phenomenon that involves a shock front followed by a reaction zone. The classical theory in detonation waves was pioneered by Zekdivich [1], von Neumann [2] and Doering [3], namely the ZND detonation model. Then both theoretical studies and numerical techniques have been developed to investigate the detonation phenomenon in many physical

* Received January 26, 2011 / Revised version received August 5, 2011 / Accepted August 10, 2011 / Published online November 15, 2011 /

applications. Numerical approaches such as PPM with front tracking and mesh refinement [4], Roe's solver with superbee limiter and the minmod limiter [5], unsplit scheme [6], and WENO-M with shock fitting [7] have been implemented to simulate detonation waves to study its instability and mechanisms.

Although detonation has been studied for many years, it remains an active area of research in both theoretical studies and in numerical simulations due to the practical importance. In this paper, we are interested in the numerical simulations of one-dimensional detonation waves by Weighted Essentially Non-Oscillation (WENO) schemes, which have been developed in recent years as a class of high order/high resolution method for solutions of hyperbolic conservation laws in the presence of shocks and small scale structures in the solution.

The local computational stencils of $(2r-1)$ order WENO schemes are composed of r overlapping substencils of r points, forming a larger stencil with $(2r-1)$ points. The scheme yields a local rate of convergence that goes from order r at the non-smooth parts of the solution, to order $(2r-1)$ when the convex combination of local lower order polynomials is applied at smooth parts of the solution. The nonlinear coefficients of WENO's convex combination, hereafter referred to as *nonlinear weights* ω_k, are based on lower order local smoothness indicators $\beta_k, k=0,\cdots,r-1$ that measure the sum of the normalized squares of the scaled L^2 norms of all derivatives of r local interpolating polynomials. An essentially zero weight is assigned to those lower order polynomials whose underlining substencils contain high gradients and/or shocks, aiming at an essentially non-oscillatory solution close to discontinuities. At smooth parts of the solution, the formal order of accuracy is achieved through the mimicking of the central upwind scheme of maximum order, when all smoothness indicators are about the same size. Hence, the one of the most important issues for WENO schemes is to design an efficient and accurate nonlinear weights ω_k. In [8], the first set of nonlinear weights of widespread use has been given. However, it has been shown that the nonlinear weights fail to satisfy the necessary and sufficient condition for achieving the formal order of accuracy even for smooth functions. We call this scheme as the classical WENO scheme (WENO-JS). In [9], a modification of the nonlinear weights was proposed in the form of a mapping on the classical WENO-JS nonlinear weights, leading to corrected nonlinear weights that recovered the formal order of accuracy. We call the scheme composed by this mapped set of nonlinear weights as the mapped WENO scheme (WENO-M). In [10], it was shown that the incorporation of a global optimal order smoothness indicator, hereafter denoted as τ_{2r-1}, into the classical WENO-JS nonlinear weights definition satisfies the necessary and sufficient condition for achieving the formal order of accuracy. This scheme has been named the WENO-Z scheme (WENO-Z). The mapping procedure of WENO-M incurs extra expensive computational cost, while the weight modification of WENO-Z is obtained through a simple and inexpensive linear combination of the already computed lower order local smoothness indicators β_k. It has been shown that the new set of nonlinear weights of WENO-Z provided less dissipation than WENO-JS and yielded comparable resolution of smooth solution and captured sharp gradients as WENO-M [10].

Numerical experiments showed that detonation waves for overdrive factor f, which is the square of the ratio of imposed detonation front velocity and the Chapman-Jouguet velocity, $f=1.8$ is a stable case and lower overdrive factors $f=1.6$, $f=1.3$ and $f=1.1$ are unstable cases. For the stable case, the temporal histories of peak pressure of the detonation front computed by WENO-JS and WENO-Z schemes reach the steady state while the temporal history of peak pressure computed by the WENO-M fails to reach the steady state. For the unstable cases, the results of three versions of WENO schemes agree well with each other as

resolution, defined as number of grid points per half-length of reaction zone, increases, except for overdrive factor $f = 1.3$ where the temporal history of peak pressure behaves slightly different. In the case of overdrive factor $f = 1.1$, which is a highly unstable case, WENO-JS, WENO-M and WENO-Z with low resolution (15 points per half-length of reaction zone) demonstrate that the explosive rise of the peak pressure occurs at time $t \approx 75$, $t \approx 70$, $t \approx 66$ respectively. In contrast, three WENO schemes with high resolution (50 points per half-length of reaction zone) demonstrate a different temporal peak pressure from those with lower resolutions. This is a well-known problem, which was called *under-resolved* simulation.

The paper is organized as follows. In Section 2, a brief introduction to three versions of WENO schemes is given. Section 3.2 outlines the general framework of numerical schemes. In Section 3, a brief introduction to detonation model with governing equations and its initial conditions is given. Numerical experiments with unstable and stable overdrive factors ($f = 1.1 - 1.8$) are simulated with different resolutions and their results are discussed in Section 4. Conclusion and future work are given in Section 5.

2. Weighted Essentially Non-Oscillation Schemes

In this section we briefly introduce the general framework of the three versions of the $(2r-1)$ order characteristics based weighted essentially non-oscillatory conservative finite difference scheme with $r \geq 3$ for solving the system of hyperbolic conservation laws in the form of

$$\frac{\partial \mathbf{u}}{\partial t} + \nabla \cdot \mathbf{F}(\mathbf{u}) = \mathbf{0}. \tag{2.1}$$

Without a lost of generalities, we will present the conservative WENO finite difference scheme in one dimension.

Consider a uniform grid defined by the points $x_i = i\Delta x, i = 0, \cdots, N$, which are called cell centers, with cell boundaries or intercell boundaries given by $x_{i+\frac{1}{2}} = x_i + \frac{\Delta x}{2}$, where Δx is the uniform grid spacing. The semi-discretized form of (2.1) is transformed into the system of ordinary differential equations by method of line

$$\frac{du_i(t)}{dt} = -\left.\frac{\partial f}{\partial x}\right|_{x=x_i}, \qquad i = 0, \cdots, N, \tag{2.2}$$

where $u_i(t)$ is a numerical approximation to the point value $u(x_i, t)$.

To form the flux differences across the uniformly spaced cells, conservative finite-difference formulation for hyperbolic conservation laws requires high-order consistent numerical fluxes at the cell boundaries. The conservative property of the spatial discretization is obtained by implicitly defining the numerical flux function $h(x)$ as

$$f(x) = \frac{1}{\Delta x}\int_{x-\frac{\Delta x}{2}}^{x+\frac{\Delta x}{2}} h(\xi)d\xi,$$

such that the spatial derivative in (2.2) is exactly approximated by a conservative finite difference formula at the intercell boundaries $x_{i\pm\frac{1}{2}}$,

$$\frac{du_i(t)}{dt} = \frac{1}{\Delta x}\left(h_{i+\frac{1}{2}} - h_{i-\frac{1}{2}}\right), \tag{2.3}$$

where $h_{i\pm\frac{1}{2}} = h(x_{i\pm\frac{1}{2}})$. High order polynomial interpolations to $h_{i\pm\frac{1}{2}}$ are computed using known grid values of $f_i = f(x_i)$. The classical $(2r-1)$ order WENO scheme uses $(2r-1)$-points

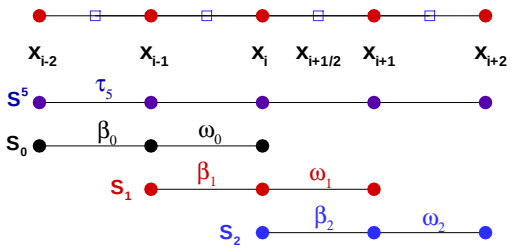

Fig. 2.1. The computational uniform grid x_i and the 5-points stencil S^5, composed of three 3-points substencils S_0, S_1, S_2, used for the fifth-order WENO reconstruction step.

global stencil, which is subdivided into r substencils $\{S_0, S_1, \cdots, S_{r-1}\}$ with each substencil containing r grid points. For the fifth-order WENO scheme ($r = 3$) the 5-points stencil, hereafter named S^5, is subdivided into three 3-points substencils $\{S_0, S_1, S_2\}$, as shown in Fig. 2.1.

The $(2r-1)$ degree polynomial approximation $\hat{f}_{i\pm\frac{1}{2}} = h_{i\pm\frac{1}{2}} + O(\Delta x^{2r-1})$ is built through the convex combination of the interpolated values $\hat{f}^k(x_{i\pm\frac{1}{2}})$, in which $f^k(x)$ is the r degree polynomial below, defined in each one of the substencils S_k:

$$\hat{f}_{i\pm\frac{1}{2}} = \sum_{k=0}^{r-1} \omega_k \hat{f}^k(x_{i\pm\frac{1}{2}}), \tag{2.4}$$

where

$$\hat{f}^k(x_{i+\frac{1}{2}}) = \hat{f}^k_{i+\frac{1}{2}} = \sum_{j=0}^{r-1} c_{kj} f_{i-k+j}, \quad i = 0, \cdots, N. \tag{2.5}$$

The c_{kj} are Lagrangian interpolation coefficients (see, e.g., [8]), which depend on the left-shift parameter $k = 0, \cdots, r-1$, but independent from the values f_i and ω_k are normalized nonlinear weights, or, simply, weights unless stated otherwise, which will be described below.

The process synthesized by (2.4)-(2.5) is called the WENO reconstruction step, for it reconstructs the values of $h(x)$ at the cell boundaries of the interval $I_i = [x_{i-\frac{1}{2}}, x_{i+\frac{1}{2}}]$ from its cell averaged values $f(x)$ in the substencils $\{S_k, k = 0, \cdots, r-1\}$.

The regularity of the $(r-1)$ degree interpolation polynomial approximation $\hat{f}^k(x)$ at the substencil S_k is measured by the lower order local smoothness indicators β_k, which are given by

$$\beta_k = \sum_{l=1}^{r-1} \Delta x^{2l-1} \int_{x_{i-\frac{1}{2}}}^{x_{i+\frac{1}{2}}} \left(\frac{d^l}{dx^l} \hat{f}^k(x) \right)^2 dx. \tag{2.6}$$

We refer to [8,10] for details of expression of the β_k in terms of the cell averaged values of f_i.

2.1. The Classical WENO Scheme (WENO-JS)

In the classical WENO scheme [8,11] (WENO-JS), the normalized nonlinear weights ω_k and un-normalized nonlinear weights α_k in each substencil S_k, are defined as

$$\omega_k = \frac{\alpha_k}{\sum_{l=0}^{r-1} \alpha_l}, \qquad \alpha_k = \frac{d_k}{(\beta_k + \epsilon)^p}, \quad k = 1, \cdots, r-1. \tag{2.7}$$

The parameter ϵ (typically 10^{-12}) is used to avoid the division by zero in the denominator and power parameter $p = 2$ is chosen to increase the difference of scales of distinct weights at non-smooth parts of the solution. The coefficients $\{d_0, d_1, \cdots, d_{r-1}\}$ are called the ideal weights since they generate the $(2r-1)$ order central upwind scheme using the $(2r-1)$-points stencil when the solution is smooth. For $r = 3$, the ideal weights are $\left\{d_0 = \frac{3}{10},\ d_1 = \frac{3}{5},\ d_2 = \frac{1}{10}\right\}$.

2.2. The Mapped WENO Scheme (WENO-M)

In the mapped WENO scheme [9] (WENO-M), it proposed a modification of the normalized nonlinear weights ω_k to address the degradation of the order of accuracy at the smooth stencil at a first order critical point x_c (where $f'(x_c) = 0, f''(x_c) \neq 0$), by applying a non-decreasing monotone function $g_k(\omega)$ to enhance the approximation of ω_k to the ideal weights d_k for smooth solution. The mapping function $g_k(\omega)$ is defined as

$$g_k(\omega) = \frac{\omega\left(d_k + d_k^2 - 3d_k\omega + \omega^2\right)}{d_k^2 + \omega\left(1 - 2d_k\right)}. \tag{2.8}$$

The resulting WENO-M scheme recovered the formal fifth-order convergence at first order critical points of a smooth solution while the order of accuracy would be reduced to third order using the classical WENO-JS scheme. The extra mapping function of the WENO-M scheme, however, costs an additional $\approx 15\% - 20\%$ more CPU time when compared to the classical WENO-JS scheme (see, e.g., [9, 10, 12] for details).

2.3. The WENO-Z Scheme

The novel idea of the WENO-Z scheme (WENO-Z) [10,12] is the modification of the β_k with higher order information obtained from a global optimal order smoothness indicator, which is denoted here by τ_{2r-1}. This new global optimal order smoothness indicator τ_{2r-1} is built using cell-averaged values in the whole S^{2r-1} stencil in the form of a linear combination of β_k, that is,

$$\tau_{2r-1} = \sum_{k=0}^{r-1} c_k \beta_k, \tag{2.9}$$

where c_k are given constants (see, e.g., [10, 12]).

The general definitions of the normalized and un-normalized nonlinear weights ω_k^z and α_k^z, respectively, are

$$\omega_k^z = \frac{\alpha_k^z}{\sum_{l=0}^{r-1} \alpha_l^z}, \quad \alpha_k^z = \frac{d_k}{\beta_k^z} = d_k\left(1 + \left(\frac{\tau_{2r-1}}{\beta_k + \epsilon}\right)^p\right), \quad k = 0, \ldots, r-1, \tag{2.10}$$

where $p \geq 1$ is the power parameter, used to enhance the relative ratio between the smoothness indicators. For $r = 3$, the global high order smoothness indicator τ_5 is

$$\tau_5 = \left|\beta_0 - \beta_2\right|. \tag{2.11}$$

The numerical results in [10] confirmed the improved performance of the modified smoothness indicators over the WENO-JS scheme in computing a higher resolution solution when solving hyperbolic PDEs with discontinuous solutions.

3. Governing Equations

The governing equations that model the one-dimensional unsteady reactive Euler equations for a perfect ideal gas coupled with an irreversible chemical reaction is

$$\frac{\partial \rho}{\partial t} + \frac{\partial (\rho u)}{\partial x} = 0, \tag{3.1a}$$

$$\frac{\partial (\rho u)}{\partial t} + \frac{\partial (\rho u^2 + P)}{\partial x} = 0, \tag{3.1b}$$

$$\frac{\partial E}{\partial t} + \frac{\partial ((E+P)u)}{\partial x} = 0, \tag{3.1c}$$

$$\frac{\partial (\rho f_1)}{\partial t} + \frac{\partial (\rho f_1 u)}{\partial x} = \dot{\omega}, \tag{3.1d}$$

where ρ is density or mass density, P is pressure, u is velocity, $0 \le f_1 \le 1$ is the reactant mass fraction. It equals unity when the reactant has not been reacted, and zero when the reaction has been completed.

The total specific energy, with an addition of energy $\rho f_1 q_0$ generated through the chemical reaction, is given by

$$E = \frac{P}{\gamma - 1} + \frac{1}{2}\rho u^2 + \rho f_1 q_0, \tag{3.2}$$

and the source term for rate of species production due to the chemical reaction is

$$\dot{\omega} = -K \rho f_1 e^{-E_a/T}, \tag{3.3}$$

where γ is the ratio of specific heat (assumed to be a constant here), q_0 is the heat-release parameter, E_a is the activation-energy parameter, and K is the pre-exponential factor (stiffness coefficient) that sets the spatial and temporal scales. The temperature is defined by

$$T = P/\rho R, \tag{3.4}$$

where R is the specific gas constant (with a suitable normalization, $R = 1$ in this study).

3.1. Initial Conditions

Adopting the notations in [14], the setup of the initial condition for solving the system (3.1) is given here. By assuming the solution of system (3.1) reaches the steady state such that the detonation wave front propagates at a constant velocity D, the steady state solution of system (3.1) satisfies the following equations:

$$\frac{\partial F(Q)}{\partial x} = S, \tag{3.5}$$

where $F(Q) = (\rho u, \rho u^2 + P, (E+P)u, \rho u f_1)$ and $S = (0, 0, 0, \dot{\omega})$.

We shall specify the steady state solution in term of the dimensionless primitive variables in unreacted zone as

$$\rho = 1,\ P = 1,\ T = 1,\ u = -D. \tag{3.6}$$

By solving the ODEs (3.5) with the boundary condition (3.6), the mass flux, momentum flux and total energy flux in the flame zone satisfy the following equations

$$\rho u = -D, \tag{3.7}$$

$$\rho u^2 + P = D^2 + 1, \tag{3.8}$$

$$\rho u \left(\frac{1}{\gamma - 1} \frac{P}{\rho} - q_0 f_2 + \frac{u^2}{2} \right) + Pu = -D \left(\frac{\gamma}{\gamma - 1} + \frac{D^2}{2} \right), \tag{3.9}$$

where $f_2 = 1 - f_1$. Using Eqs. (3.7) and (3.8), Eq. (3.9) becomes

$$\frac{1}{2}u^2 + \frac{\gamma}{\gamma + 1} \left(D + \frac{1}{D} \right) u + \frac{\gamma - 1}{\gamma + 1} \left(q_0 f_2 + \frac{\gamma}{\gamma - 1} + \frac{1}{2} D^2 \right) = 0. \tag{3.10}$$

This is a quadratic equation of u and its solutions are

$$u_{\pm} = -\frac{\gamma}{\gamma - 1} \left(D + \frac{1}{D} \right) \pm \sqrt{\xi(f_2)}, \tag{3.11}$$

where

$$\xi(f_2) = \left[\frac{\gamma}{\gamma + 1} \left(D + \frac{1}{D} \right) \right]^2 - 2 \frac{\gamma - 1}{\gamma + 1} \left(q_0 f_2 + \frac{\gamma}{\gamma - 1} + \frac{1}{2} D^2 \right). \tag{3.12}$$

Eq. (3.10) has two roots (3.11), but the one with negative sign does not exist in most situations; thus we choose the one with positive sign.

Furthermore, by assuming $\xi(f_2) = 0$ in Eq. (3.12), the upper Chapman-Jouguet velocity D_{CJ}^2 is determined as

$$D_{CJ}^2 = \left[\gamma + (\gamma^2 - 1) q_0 \right] + \sqrt{\left[\gamma + (\gamma^2 - 1)\, q_0 \right]^2 - \gamma^2}, \tag{3.13}$$

which is the minimum speed for ZND profile.

Hence, the detonation wave velocity D becomes

$$D^2 = f D_{CJ}^2, \tag{3.14}$$

where the non-dimensional parameter $f \geq 1$ is the overdrive factor of detonation.

Giving the parameters γ and q_0, the C-J velocity D_{CJ} can be readily obtained by using Eq. (3.13). Then by specifying the overdrive factor f, the detonation velocity D can be determined. Finally, the primitive variables u, ρ and P for a given mass fraction f_1 can be computed via Eqs. (3.7), (3.8) and (3.11). We refer to [14] for details.

In this study, the initial spatial profile of the mass fraction f_1 is specified via an exponential function

$$f_1(x) = \begin{cases} 0, & x \leq x_0 - L_{1/2}, \\ \exp\left\{ -\alpha \left(\frac{x_0 + 2L_{1/2}}{4L_{1/2}} - x \right)^k \right\}, & x_0 + L_{1/2} > x > x_0 - L_{1/2}, \\ 1, & x \geq x_0 + L_{1/2}, \end{cases} \tag{3.15}$$

where $\alpha = -\ln(\varepsilon)$, ε is the machine zero, x_0 is the location of the detonation front and $L_{1/2}$ is the half-length of reaction zone. We choose $k = 2.8505$ such that $f_1(x_0) \approx 0.5$ and $L_{1/2} = 1$ in the following numerical experiments.

The typical ZND spatial profiles of the mass fraction f_1, pressure P, velocity u and density ρ are shown in Fig. 3.1. These profiles will be used as the initial condition of the detonation simulations that follow. Since the one-dimensional computational domain is specified sufficient large to contain all the flow structures, the boundary conditions at both ends of the domain are set to their respective free-stream conditions.

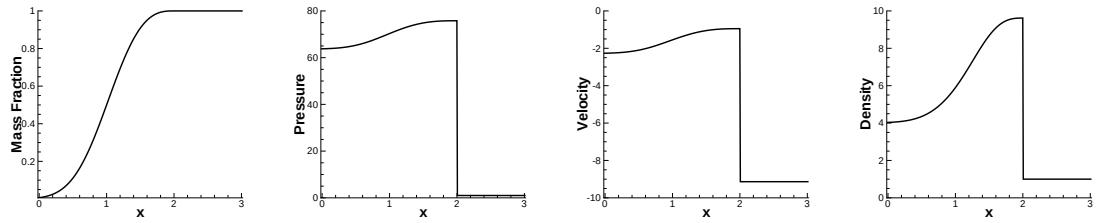

(a) (b) (c) (d)

Fig. 3.1. Typical profiles of (a) mass fraction f_1, (b) pressure P, (c) velocity u, and (d) density ρ for a one-dimensional ZND detonation wave.

3.2. Numerical Methods

We will employ the characteristics based WENO conservative finite difference scheme for system of hyperbolic conservation laws (in this case, one-dimensional Euler equation). We approximate the inviscid flux, which is the classical Euler equations, via the well known $(2r-1)$ order characteristic-based weighted essentially non-oscillatory conservative finite difference scheme (WENO) explicitly. Following [8,10,11], the hyperbolicity of the Euler equations admits a complete set of right and left eigenvectors for the Jacobian of the system (see Appendix 5 for details). The approximated eigenvalues and eigenvectors are obtained via the Roe linearized Riemann solver [13]. The first order global Lax-Friedrichs flux is used as the low order building block for the high order reconstruction step of the WENO scheme. After projecting the positive and negative fluxes on the characteristic fields via the left eigenvectors, the high order WENO reconstruction step is applied to obtain the high order approximation at the cell boundaries using the surrounding cell-centered values, which are then projected back into the physical space via the right eigenvectors and added together to form a high order numerical flux at the cell-interfaces. The conservative difference of the reconstructed high order fluxes can then be computed for inviscid flux.

The resulting set of ODE (2.3) is advanced in time via the third order TVD Runge-Kutta scheme [8]. The CFL condition is set to be CFL = 0.4 in the numerical experiments performed in this study. We refer to [8, 10] for further details on the WENO algorithm for solving the hyperbolic conservation laws.

4. Numerical Experiments and Discussion

According to the linear stability analysis [15] of the conservation system (3.1), there is a large range of the parameters γ, q_0, E_a and f to make the detonation system unstable. In the numerical experiments below, we use the following parameters

$$\gamma = 1.2,\ q_0 = 50,\ E_a = 50. \tag{4.1}$$

Therefore, the stability of detonation system is determined by the overdrive factor f only. The linear stability analysis shows that there is a critical value $f_c = 1.72$ which determines the stability of the conservation system (3.1). The system is stable for the overdrive factor $f \geq f_c$ and unstable for $f < f_c$ [4].

In the following, we evaluate the performance of the three versions of WENO scheme on one stable (overdrive factor $f = 1.8$) and three unstable (overdrive factor $f = 1.6$, $f = 1.3$,

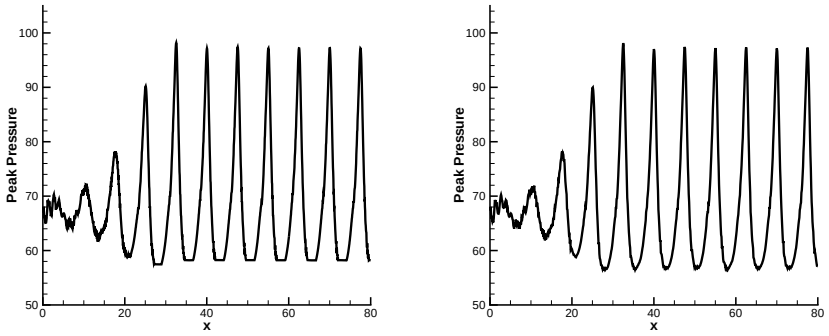

(a) Full domain (b) Reaction zone only

Fig. 4.1. The peak pressure temporal histories $P_m(t)$ of WENO-Z scheme measured in (a) Full domain and (b) Reaction zone only. 'Clipping' of the pressure profile occurs when measure the pressure maximum on the entire computational domain.

$f = 1.1$) one-dimensional detonation waves, all of which have been studied with different numerical techniques (most of them are low order schemes). As the common practice, we define the resolution δ_n as the number of grid points in the half-reaction length $L_{1/2}$. The size of computation domain and the location of detonation front are calculated approximately when the overdrive factor f and the final time t_f are given.

The peak pressure $P_m(t)$, which is the maximum pressure at the precursor explosion in the ZND wave as a function of time, is regarded as an important physical quantity for detonation analysis [4]. Additionally, it is used to validate the performance of different numerical schemes. To measure peak pressure, one should aware that the global maximum pressure of the whole domain will result in a 'clipped' peak pressure profile, as shown in Fig. 4.1. We refer to [16] for details.

Therefore, the maximum of the pressure measured in the reaction zone is used in the following numerical experiments unless stated otherwise.

4.1. Stable Detonation

We first simulate a stable detonation with the overdrive factor $f = 1.8$ and the final time $t_f = 50$. The detonation front speed and stiffness coefficient are $D = 9.1359$ and $K = 145.69$ respectively. The peak pressure temporal histories $P_m(t)$ at two resolutions are shown in Fig. 4.2. In both cases of δ_{15} and δ_{30}, the performance of WENO-JS and WENO-Z are quantitatively and qualitatively similar. The results converge to the peak pressure of steady state solution for $t > 20$, which agrees well with results in [4, 6]. However, the peak pressure temporal history $P_m(t)$ computed by WENO-M oscillates around the steady state solution with low resolution δ_{15} and still unable to reach the steady state solution with high resolution δ_{30}.

4.2. Unstable Detonation

In this section, we shall consider a few more interesting unstable cases with overdrive factors $f = 1.6$, $f = 1.3$ and $f = 1.1$.

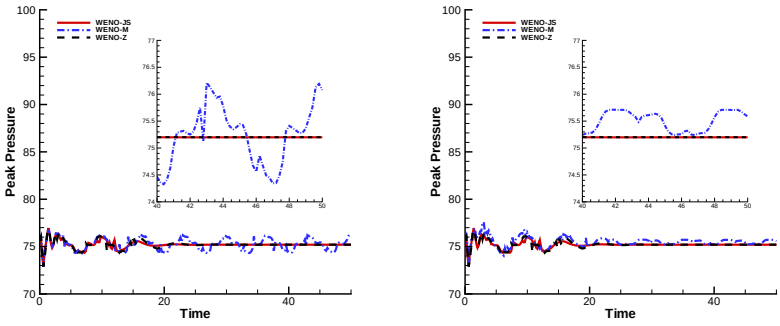

(a) $f = 1.8, \delta_{15}$ (b) $f = 1.8, \delta_{30}$

Fig. 4.2. The peak pressure temporal histories $P_m(t)$ of detonation with overdrive factor $f = 1.8$ and resolutions (a) δ_{15} and (b) δ_{30}. The insert figures show the zoom-in solution at late time.

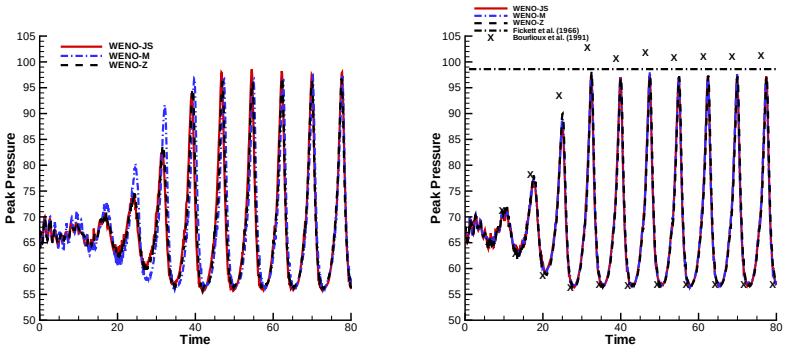

(a) $f = 1.6, \delta_{10}$ (b) $f = 1.6, \delta_{20}$

Fig. 4.3. The peak pressure temporal histories $P_m(t)$ of detonation with overdrive factor $f = 1.6$ and resolutions (a) δ_{10} and (b) δ_{20}.

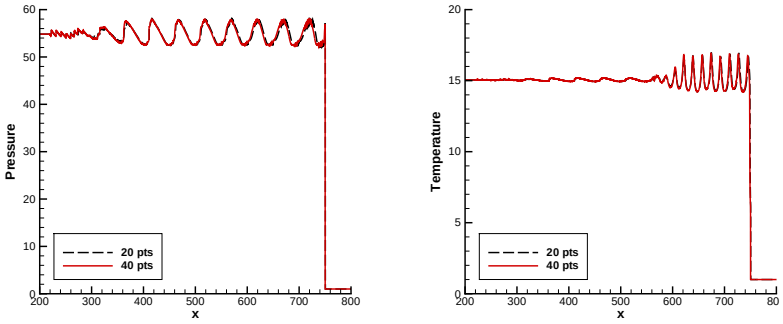

$f = 1.6,\ t = 80$

Fig. 4.4. (Left) Pressure and (Right) temperature spatial profiles with overdrive factor $f = 1.6$ at time $t = 80$. Black dashed lines: Resolution δ_{20}. Red lines: Resolution δ_{40}.

- $f = 1.6$

For the overdrive factor $f = 1.6$, the detonation front speeds and stiffness coefficients are $D = 8.6134$ and $K = 233.75$ respectively. The peak pressure temporal histories $P_m(t)$ under different resolutions are shown in Fig. 4.3. For low resolution δ_{10}, the result of WENO-M scheme

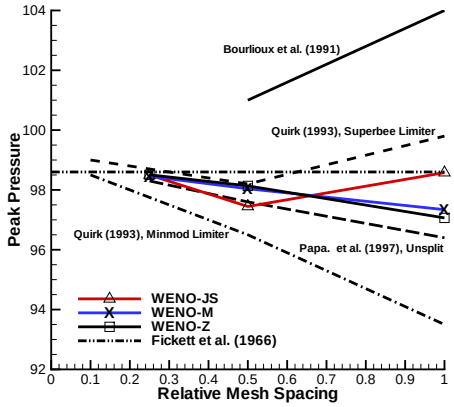

Fig. 4.5. Grid convergence study with various numerical schemes with the mildly unstable case (overdrive factor $f = 1.6$). The predicted value $P_{\max} = 98.6$.

is different from those of WENO-JS scheme and WENO-Z scheme for $t < 40$. As the resolution increases with δ_{40}, three versions of WENO schemes behave similarly and all the results oscillate periodically for $t > 33$. The results agree well with those in the literature [6]. To further verify the accuracy of WENO schemes, we compare the results in [4] and the predicted peak pressure ($P_{\max} = 98.6$) in [17] with WENO schemes with resolution δ_{20}. The peak pressure temporal histories $P_m(t)$ computed by the three WENO schemes agreed very well with the predicted peak pressure in [17] and in general good agreement with the computed peak pressure in [4]. The pressure and temperature spatial profiles computed by the WENO-Z scheme with resolutions δ_{20} and δ_{40} at the time $t = 80$ are given in the Fig. 4.4. The results of the WENO-M scheme and WENO-JS scheme are similar as the WENO-Z scheme. Their figures are omitted here to avoid clustering of the paper with similar figures.

Following [5, 6], we perform a grid convergence study for the peak pressure with the three WENO schemes along with the existing results computed with different numerical schemes. The results are summarized in Fig. 4.5. The numerical schemes used were PPM with front tracking and mesh refinement [4], unsplit scheme [6], Roe's solver with minmod limiter [5] and Roe's solver with superbee limiter [5]. In the relative grid spacing in this figure, 1 and 0.25 correspond to the resolutions δ_{10} and δ_{40} respectively. It can be seen that the WENO schemes tend to approach the predicted value obtained from linear stability analysis [17] faster than the low order schemes.

- $f = 1.3$

The overdrive factor $f = 1.3$ corresponds to $D = 7.764$ and $K = 583.71$. With low resolution δ_{20}, the peak pressure temporal histories $P_m(t)$ become irregular at $t > 33$ and more oscillatory than the above cases. General behaviors of solutions from all three WENO schemes are similar but differ slightly at high resolution δ_{40} as shown in Fig. 4.6.

The pressure and temperature spatial profiles computed by the WENO-Z scheme with resolution δ_{20} and δ_{40} at the time $t = 100$ are given in the Fig. 4.7.

- $f = 1.1$

The overdrive factor $f = 1.1$ corresponds to $D = 7.1418$ and $K = 1389.58$ in this strongly unstable case. The local and global temporal histories $P_m(t)$ of the peak pressure shows no

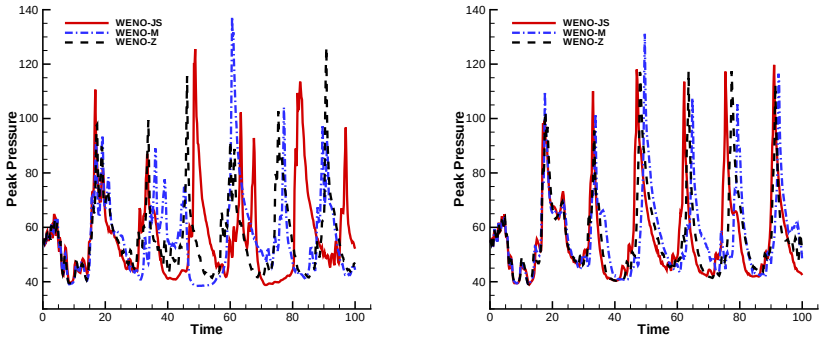

(a) $f = 1.3, \delta_{20}$ (b) $f = 1.3, \delta_{40}$

Fig. 4.6. The peak pressure temporal histories $P_m(t)$ of detonation with $f = 1.3$ with resolution (a) δ_{20} and (b) δ_{40}.

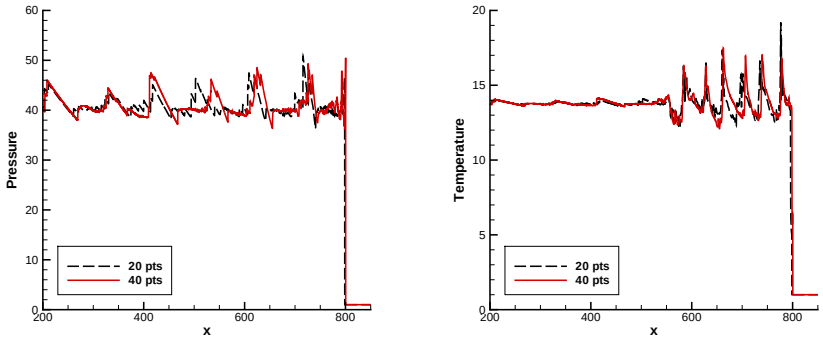

$f = 1.3,\ t = 100$

Fig. 4.7. (Left) Pressure and (Right) temperature spatial profiles with overdrive factor $f = 1.3$ at time $t = 100$. Black dashed lines: Resolution δ_{20}. Red lines: Resolution δ_{40}.

regular structures as shown in Fig. 4.8 with different resolution. At resolution δ_{15}, the local peak pressure temporal histories $P_m(t)$ computed by the three WENO schemes as shown in Fig. 4.8(a) are similar to the one shown in [6]. However, the three WENO schemes exhibit an explosive solution at different times with $P_{\max} \approx 360$ at $t \approx 66$ for WENO-Z, $P_{\max} \approx 280$ at $t \approx 70$ for WENO-M, $P_{\max} \approx 240$ at $t \approx 75$ for WENO-JS. At resolution δ_{50}, the local peak pressure temporal histories $P_m(t)$ computed by the three WENO schemes are shown in Fig. 4.8(b) behave differently at time $60 \leq t \leq 80$. The global peak pressure temporal histories $P_m(t)$ as shown in Fig. 4.8(c) and Fig. 4.8(d) demonstrate that explosive behavior of all WENO schemes happens twice at resolution δ_{15} and δ_{50}, respectively. That is, the peak pressure is generated outside of the reaction zone and the local peak pressure temporal histories $P_m(t)$ fails to capture the peak pressure outside the front zone. Moreover, all three WENO schemes behave differently with low resolution and high resolution because, in the strongly unstable cases, different resolutions are equivalent to different initial conditions. The pressure and temperature spatial profiles computed by the WENO-Z scheme with resolution δ_{15} and δ_{50} at the time $t = 100$ are given in the Fig. 4.9.

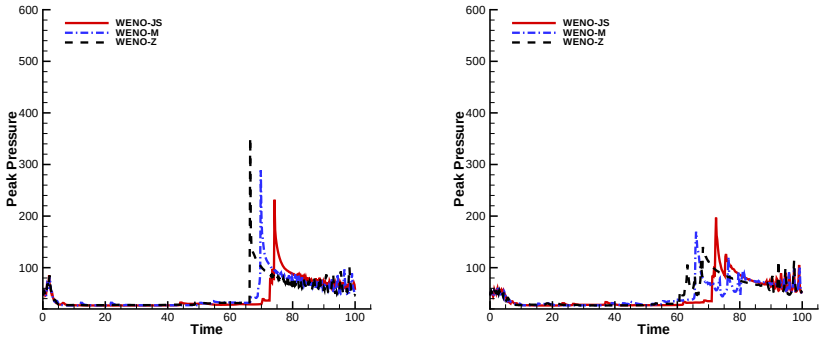

(a) $f = 1.1, \delta_{15}$ (b) $f = 1.1, \delta_{50}$

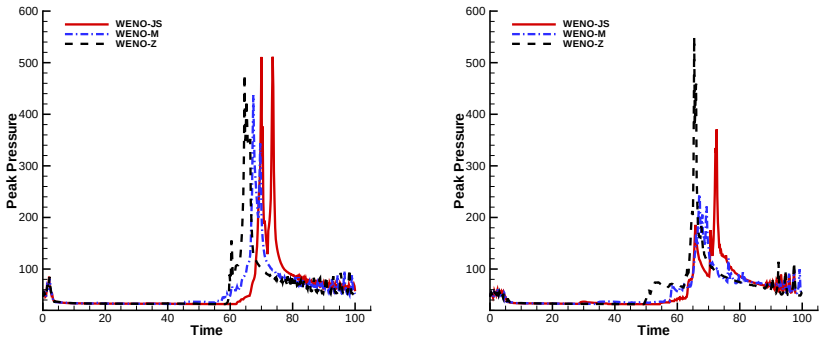

(c) $f = 1.1, \delta_{15}$ (d) $f = 1.1, \delta_{50}$

Fig. 4.8. The local peak pressure temporal histories $P_m(t)$ of detonation with $f = 1.1$ with resolution (a) δ_{15} and (b) δ_{50}. The global peak pressure temporal histories $P_m(t)$ of detonation with $f = 1.1$ with resolution (c) δ_{15} and (d) δ_{50}.

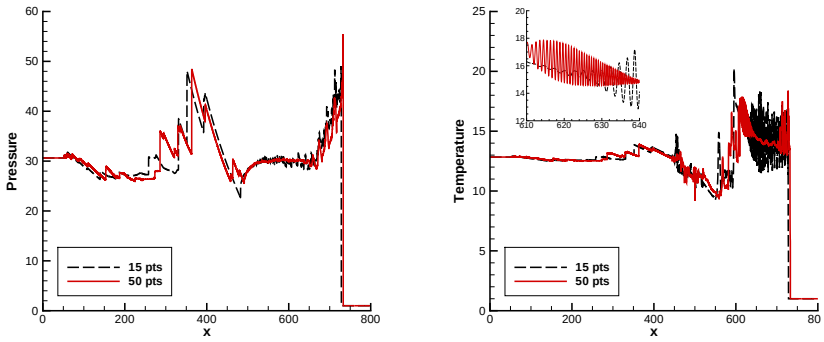

$f = 1.1,\ t = 100$

Fig. 4.9. (Left) Pressure and (Right) temperature spatial profiles with overdrive factor $f = 1.1$ at time $t = 100$. Black dashed lines: Resolution δ_{15}. Red lines: Resolution δ_{50}.

Remark. In [4], it was proposed the existence of chaotic-pulsation instabilities because of the results sensitively depended on the initial data. Numerical experiments are performed with a perturbation on the ZND profiles of the fluid-dynamic variables with certain unity length

for lower value of overdrive factors $f = 1.3$ and $f = 1.1$. These initial small perturbations aim at investigating the typical behaviors for chaotic system with small number of degree of freedom [4].

5. Conclusion and Future Work

In this work, we presented some preliminary numerical study of one dimensional detonation wave simulations. The governing equations are a system of nonlinear hyperbolic conservation laws with a species production source term based on a simple irreversible chemical reaction. To solve the nonlinear hyperbolic system, we employed the high order weighted essentially nonscillatory finite difference scheme and high order TVD Runge-Kutta scheme in order to capture sharp detonation fronts and to resolve small scales structures that appear in the highly complex solution of PDEs. More specifically, the performance of three versions of fifth order characteristic based WENO finite difference schemes, namely, the classical WENO scheme (WENO-JS), the mapped WENO scheme (WENO-M) and the improved WENO scheme (WENO-Z) are studied for both the stable and unstable cases of detonation. The numerical code is written using the subroutines in the high performance software library WENOpack [18].

For the stable detonation with overdrive factor $f = 1.8$, the computed peak pressure in time reaches the theoretical steady state when computed by the WENO-JS and WENO-Z schemes. However, the WENO-M scheme failed to reach and oscillate around the theoretical steady state even though the detonation is stable. It is indicative that the WENO-JS and WENO-Z schemes are a better choice than the WENO-M scheme for this class of problems. For the mildly unstable detonation with overdrive factor $f = 1.6$, the peak pressure exhibits a steady and stable oscillatory behavior in time. The three WENO schemes agreed well with each other with an increased resolution. Moreover, the grid convergence study with overdrive factor $f = 1.6$ shows that the high order WENO schemes converges to the predicted peak pressure faster than the lower order schemes such as unsplit scheme, Roe's solver with minmod limiter and Roe's solver with superbee limiter. For strongly unstable detonation with overdrive factors $f = 1.3$ and $f = 1.1$, the solutions of the system exhibit an increased chaotic behavior along with sudden strong explosive growth of the peak pressure with similar results appeared in the literature. Also we examined the spatial profiles of the pressure and the temperature computed by the WENO-Z scheme at low and high resolutions.

In our future work in this area, we are interested in extending the methodology of high order numerical methods for simulating two and three dimensions problems in detonation with increasingly realistic chemical reactions and chemical species. We will examine quantitative behavior of the system via the mixing profile, statistics and spectra of perturbation energy fields (see, e.g., [19]).

Acknowledgments. The authors would like to acknowledge the funding support of this research by the RGC grant HKBU-200910 from Hong Kong University Grant Council. The first author gratefully acknowledges the invitation of Prof. W.-S. Don, and also extends his gratitude to the Department of Mathematics at Hong Kong Baptist University for hosting his visit. He also acknowledges Prof. Cheng Wang for many useful discussions throughout the research and the funding support of this research by the Fundamental Research Funds for the Central Universities (1501-841111012).

Appendix

Eigensystem of the Reactive Euler Equations

For the homogeneous system of (3.1), the Jacobian matrix of the Euler flux is,

$$\mathbf{A}(\mathbf{Q}) = \begin{bmatrix} 0 & 1 & 0 & 0 \\ \frac{1}{2}(\gamma-3)u^2 & (3-\gamma)u & (\gamma-1) & (1-\gamma)q_0 \\ (\gamma-1)(q_0 f_1 u + u^3) - \frac{\gamma u E}{\rho} & \frac{\gamma E}{\rho} - (\gamma-1)(q_0 f_1 + \frac{3}{2}u^2) & \gamma u & (1-\gamma)q_0 u \\ u f_1 & f_1 & 0 & u \end{bmatrix}.$$

The right and left eigenvector matrices $\mathbf{R}$ and $\mathbf{R^{-1}}$ of $\mathbf{A}$, respectively, are

$$\mathbf{R} = \begin{pmatrix} 1 & 1 & 2 & -2q_0 \\ u+c & u-c & 2u & -2uq_0 \\ h+cu & h-cu & u^2 & 0 \\ f_1 & f_1 & 0 & u^2 \end{pmatrix},$$

$$\mathbf{R^{-1}} = \begin{pmatrix} \frac{(\gamma-1)u^2-2cu}{4c^2} & -\frac{(\gamma-1)u-c}{2c^2} & \frac{\gamma-1}{2c^2} & -\frac{(\gamma-1)q_0}{2c^2} \\ \frac{(\gamma-1)u^2+2cu}{4c^2} & -\frac{(\gamma-1)u+c}{2c^2} & \frac{\gamma-1}{2c^2} & -\frac{(\gamma-1)q_0}{2c^2} \\ \frac{2c^2-(\gamma-1)h}{2c^2} & \frac{(\gamma-1)h-c^2}{uc^2} & \frac{c^2-(\gamma-1)h}{u^2c^2} & \frac{(\gamma-1)hq_0}{u^2c^2} \\ -\frac{(\gamma-1)f_1}{2c^2} & \frac{(\gamma-1)f_1}{uc^2} & -\frac{(\gamma-1)f_1}{u^2c^2} & \frac{(2h-u^2)(\gamma-1)}{2u^2c^2} \end{pmatrix},$$

and the corresponding eigenvalues are,

$$\lambda_1 = u+c,\ \lambda_2 = u-c,\ \lambda_3 = u,\ \lambda_4 = u,$$

where $h = (E+P)/\rho$ and $c = \sqrt{\gamma P/\rho}$ are *specific enthalpy* and *sound speed*.

References

[1] Y.B. Zeldovich, On the theory of the propagation of detonation in gaseous system, *Zh. Eksp. Teor. Fiz.*, **10** (1940), 542–568.

[2] J. von Neumann, Theory of Detonation Waves, John von Neumann, Collected Works, Macmillan, New York, **6** (1942).

[3] W. Doering, On detonation processes in gases, *Ann. Phys.*, **43** (1943), 421–436.

[4] A. Bourlioux, A.J. Majda and V. Roytburd, Theoretical and numerical structure for unstable one-dimensional detonations, *SIAM J. Appl. Math.*, **51** (1991), 303–343.

[5] J.J. Quirk, Godunov-type schemes applied to detonation flows, *ICASE Report*, **93** 15 (1993).

[6] M.V. Papalexandris, A. Leonard and P.E. Dimotakis, Unsplit schemes for hyperbolic conservation laws with source terms in one space detonation, *J. Comput. Phy.*, **134** (1997), 31–61.

[7] A.K. Henrick, T.D. Aslam and J.M. Powers, Simulations of pulsating one-dimensional detonations with true fifth order accuracy, *J. Comput. Phys.*, **213** (2006), 311–329.

[8] G.S. Jiang and C.W. Shu, Efficient Implementation of Weighted ENO Schemes, *J. Comput. Phys.*, **126** (1996), 202–228.

[9] A.K. Henrick, T.D. Aslam and J.M. Powers, Mapped weighted essentially non-oscillatory schemes: Achieving optimal order near critical points, *J. Comput. Phys.*, **207** (2005), 542–567.

[10] R. Borges, M. Carmona, B. Costa and W.S. Don, An improved weighted essentially non-oscillatory scheme for hyperbolic conservation laws, *J. Comput. Phys.*, **227** (2008), 3101–3211.

[11] D. Balsara and C.W. Shu, Monotonicity preserving weighted essentially non-oscillatory schemes with increasingly high order of accuracy, *J. Comput. Phys.*, **160** (2000), 405–452.
[12] M. Castro, B. Costa and W.S. Don, High order weighted essentially non-oscillatory WENO-Z schemes for hyperbolic conservation laws, *J. Comput. Phys.*, **230** (2011), 1766–1792.
[13] E.F. Toro, Riemann Solvers and Numerical Methods for Fluid Dynamics, A Practical Introduction, Springer, 1999.
[14] Z.C. Zhang, S.T. Yu, H. He and S.C. Chang, Direct calculation of two- and three- dimensional detonations by an extended CE/SE method, *AIAA*, (2001), 2001–0476.
[15] H.I. Lee and D.S. Stewart, Calculation for linear detonation instability: one-dimensional instability of plane detonation, *J. Fluid Mech.*, **206** (1990), 103–132.
[16] P. Hwang, R.P. Fedkiw, B. Merriman, T.D. Aslam, A.R. Karagozian and S.J. Osher, Numerical resolution of pulsating detonation waves, *Combust. Theor. Model.*, **4** (2000), 217–240.
[17] W. Fickett and W.W. Wood, Flow calculation for pulsating one-dimensional detonation, *Phys. Fluids*, **9** (1966), 903–916.
[18] W.S. Don, WENOpack, *http://www.math.hkbu.edu.hk/∼wsdon/*.
[19] M. Latini, O. Schilling and W.S. Don, Effects of order of WENO flux reconstruction and spatial resolution on reshocked two-dimensional Richtmyer-Meshkov instability, *J. Comput. Phys.*, **221** (2007), 805–836.